A 100-Mb/s Current-to-Current Galvanic-Coupling-Communication TX/RX Achieving 0.94-pJ/b TX Energy Efficiency for Neural Implant Systems

Hyunyeop Lee*[1], Dongyoon Lee*[1], Yunchul Chung[1], Sohmyung Ha[2], and Minkyu Je[1]
*Equally Credited Authors
[1]School of Electrical Engineering, Korea Advanced Institute of Science and Technology (KAIST), Daejeon, South Korea
[2]Division of Engineering, New York University Abu Dhabi, Abu Dhabi, United Arab Emirates
Email: hyl@kaist.ac.kr; mkje@kaist.ac.kr

***Abstract*—This work presents a novel galvanic-coupling-communication (GCC) method, ITX-IRX GCC, which transmits and receives current to achieve high channel gain over a wide frequency bandwidth and high energy efficiency. In-vitro measurement using porcine tissue confirms reliable communication, achieving a bit-error rate lower than 10^{-6} through 10-mm and 15-mm tissue layers with a 3-cm electrode pitch. Fabricated using a 65-nm CMOS process, the IC achieves a TX energy efficiency of 0.94 pJ/b at a data rate of 100 Mb/s, making it highly suitable for uplink communication in implantable systems.**

***Index Terms*—Current-to-current communication, galvanic-coupling communication, ultra-low-power transmitter, transimpedance amplifier, implantable devices.**

I. Introduction

Neural implant systems have been gaining attention due to their potential to restore and enhance human functionality. Among these, active endoskeleton systems, fully implantable with integrated actuators, require uplink data rates of tens of Mb/s to transmit multi-channel neural recording signals, electromyography (EMG) signals, and pressure sensor signals, essential for precise motion feedback. Moreover, minimizing power consumption in the uplink TX is critical for reducing heat generation and battery-dominant device volume.

Fig. 1 shows prior wireless communications for neural implants. RF-based communications allow high data rates but suffer from high tissue attenuation [1], [2]. Body-channel communication (BCC), which uses the human body as its transmission medium, has emerged as a promising alternative. However, capacitive-coupling BCC (CC-BCC) faces significant path loss due to reduced return-path capacitance in implanted conditions [3]. Galvanic-coupling communication (GCC) also has challenges. Voltage-transmitting and voltage-receiving (VTX-VRX) GCC suffers from signal loss due to unregulated current flowing through low-impedance paths in the body [4], [5], which can also pose a safety issue in implantable scenarios. Meanwhile, current-transmitting and voltage-receiving (ITX-VRX) GCC transmits regulated current, and the signal is received as the voltage across a 100 Ω termination resistor [6]. While this approach enhances channel bandwidth over 100 MHz, the termination resistance leads to lower channel gain and degraded RX sensitivity.

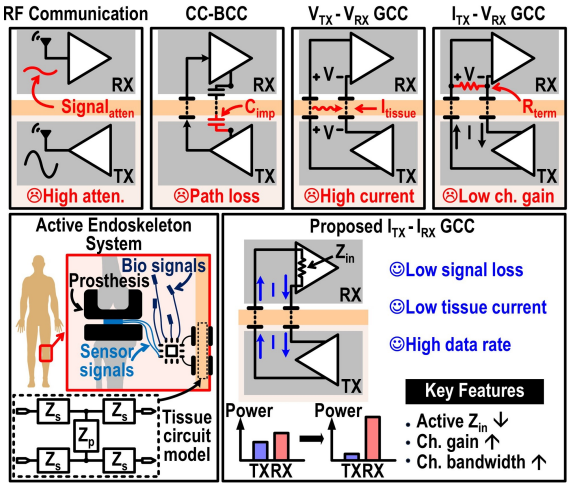

Fig. 1. Prior wireless communications for neural implants and the concept of the proposed current-transmitting and current-receiving GCC with its application to an active endoskeleton system.

In this work, we propose current-transmitting and current-receiving (ITX-IRX) GCC (Fig. 1), which addresses the limitations of existing methods. In ITX-IRX GCC, a regulated current is transmitted, and the signal is received, not as a voltage across a body impedance or a passive termination resistor but as a current entering a common-gate (CG) input stage with active low-input impedance. As the input impedance decreases, the channel bandwidth increases and the channel current gain also improves. Furthermore, employing a CG input stage for current receiving, rather than a passive resistor, improves RX sensitivity, consistent with the common preference for transimpedance amplifiers (TIAs) over passive resistors in current-input topologies.

This approach achieves low signal loss, low tissue leakage current, and a high maximum data rate while significantly enhancing the implant TX's energy efficiency, making it highly suitable for the uplink communication of implantable systems.

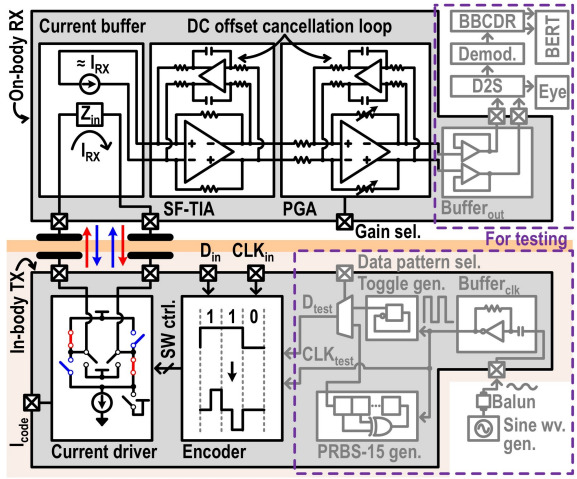

Fig. 2. Block diagram of the current-transmitting wireless neural implant TX and external current-receiving RX.

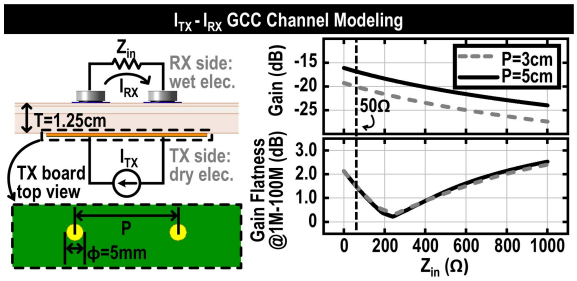

Fig. 3. ITX-IRX GCC channel model and simulated channel characteristics.

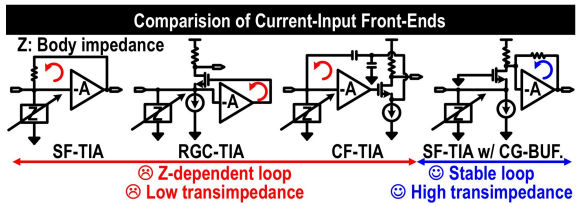

Fig. 4. Topology comparison of current-input front-end stages.

II. Proposed Architecture and Circuit Implementation

The overall block diagram of the proposed ITX-IRX GCC TX and RX is shown in Fig. 2. On the TX side, the test data pattern is selectable between a toggle pattern and a PRBS-15 pattern. The encoder processes non-return-to-zero (NRZ) data and generates control codes, enabling the current driver to transmit bipolar return-zero (B-RZ) current signals through the body channel. On the RX side, the transmitted current is received by a current buffer with unity gain and low input impedance (Z_{in}), then amplified and converted to voltage using a shunt-feedback transimpedance amplifier (SF-TIA).

Fig. 3 illustrates the channel model of the ITX-IRX GCC and simulated channel characteristics. The RX is modeled with wet electrodes, while the TX uses dry electrodes with a 5-mm diameter. Simulations were performed for electrode pitches (P) of 3 cm and 5 cm and tissue thickness (T) of 1.25 cm. The results show that the channel gain is inversely proportional to Z_{in}. At high Z_{in}, the channel exhibits low-pass filter (LPF) characteristics. As the Z_{in} decreases from 1 kΩ, the channel

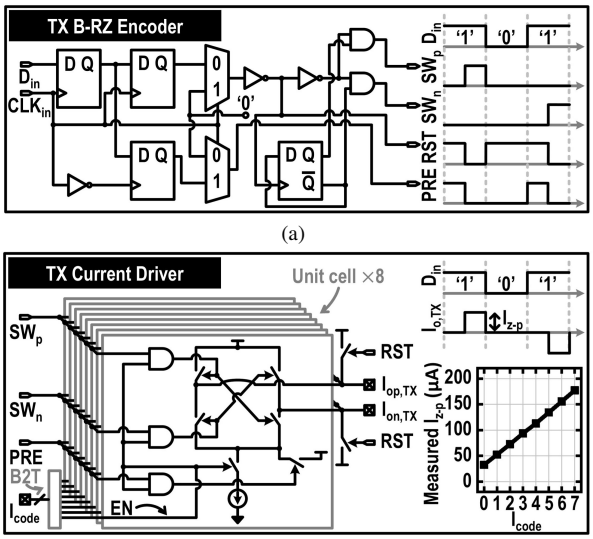

(a)

(b)

Fig. 5. (a) Circuit details of the TX's bipolar-return-zero encoder with its timing diagram. (b) TX's current driver with the measured amplitude of the output current pulse for different control code values.

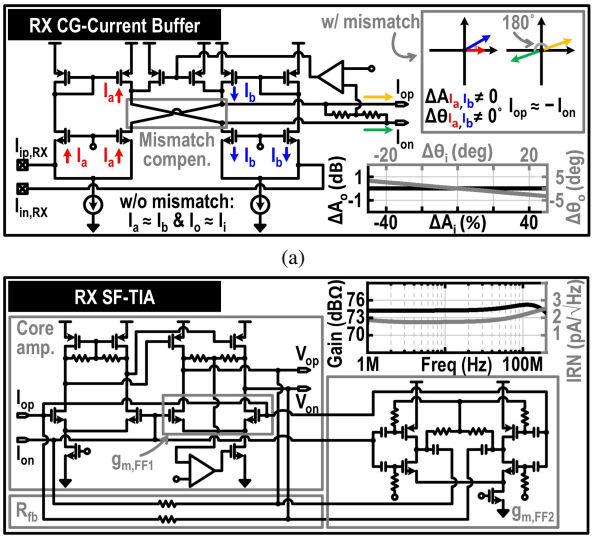

(a)

(b)

Fig. 6. (a) Circuit details of RX's CG-current buffer with amplitude and phase mismatch simulation results. (b) RX's SF-TIA with gain and input-referred noise simulation results.

becomes flatter, with the gain flatness (the difference between the maximum and minimum gain in dB) approaching 0 dB near 200 Ω. Further reduction in Z_{in} increases the high-frequency gain of the channel, and when Z_{in} approaches 0 Ω, the channel is simulated to exhibit a gain flatness of approximately 2 dB. To achieve both high channel gain and wide channel bandwidth, a 50-Ω RX Z_{in} is selected.

In closed-loop TIAs, the body impedance included within the loop makes it difficult to satisfy the stability condition. Moreover, they have the drawback of a low transimpedance limit when operating with human body, which typically exhibits low impedance. To address these challenges, the RX current-input front-end adopts an open-loop, unity-current-gain buffer followed by an SF-TIA, as shown in Fig. 4.

Fig. 5 shows the circuit details and timing diagram of the TX encoder and current driver [6]. For an NRZ signal of '1', the current driver alternates bipolar current pulses, while no current is transmitted for '0'. The transmitted current amplitude ($I_{z\text{-}p}$), controlled by the number of activated unit cells according to the I_{code} value, ranges from approximately 40 µA to 170 µA. Fig. 6 shows the circuit details of the RX current buffer (Fig. 6. (a)) and SF-TIA (Fig. 6. (b)). The current buffer features low input impedance, high output impedance, and unity current gain. By incorporating the current buffer, the input of the SF-TIA is decoupled from the body impedance, enabling the SF-TIA to achieve both high transimpedance gain and loop stability. The current buffer employs a mismatch compensation technique [7]. This mitigates the effects of differential input current mismatches, caused by either electrode contact mismatches or device mismatches. Since the current buffer provides unity current gain, the SF-TIA's high transimpedance gain and low input-referred noise (IRN) are crucial for minimizing the overall noise at the RX front-end. A feedforward amplifier with a unity-gain bandwidth (UGBW) of approximately 3 GHz is used to meet the aforementioned requirements [8].

III. Measurement Results

Fig. 7 shows the electrical measurement results of the RX circuit. The measured overall transimpedance gain of the RX is approximately 77 dBΩ in minimum gain mode and 100 dBΩ in maximum gain mode (Fig. 7. (a)). The measured integrated IRN (from 1 MHz to 200 MHz) is around 300 nA_{rms} (Fig. 7. (b)), and the measured Z_{in} value is close to 50 Ω (Fig. 7. (c)). Fig. 8 shows the in-vitro measurement setup using two types of TX boards to test different P values of 3 cm and 5 cm. The RX side uses commercial wet electrodes (Adafruit, H124SG Covidien) attached to the porcine skin. Fig. 9 shows the transmitted and received waveforms for a PRBS-15 data stream. The RX output exhibits the B-RZ signal corresponding to the digital data stream transmitted at the TX side. With T = 10 mm and P = 5 cm, the measured channel gain is approximately –17 dB, calculated from the measured values of the TX output current amplitude, RX transimpedance gain, and RX output voltage amplitude. This shows good agreement with the simulation results based on the channel model.

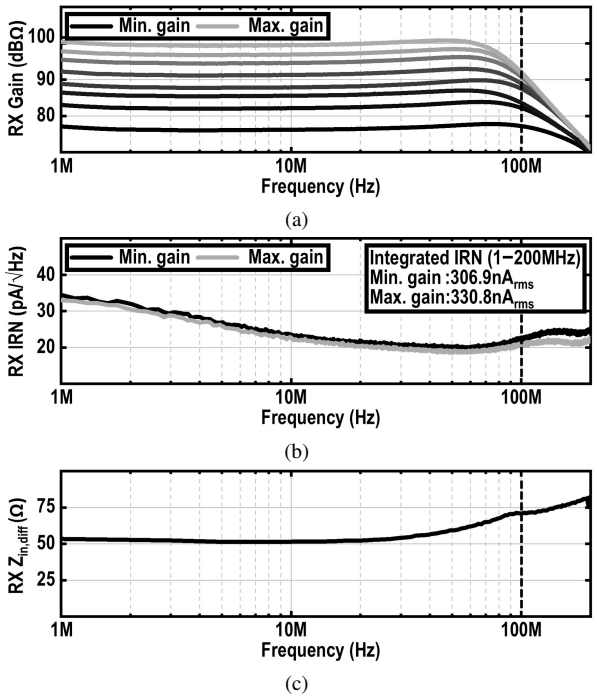

Fig. 7. Electrical measurement results: (a) measured RX gain, (b) RX input-referred noise, and (c) RX input impedance.

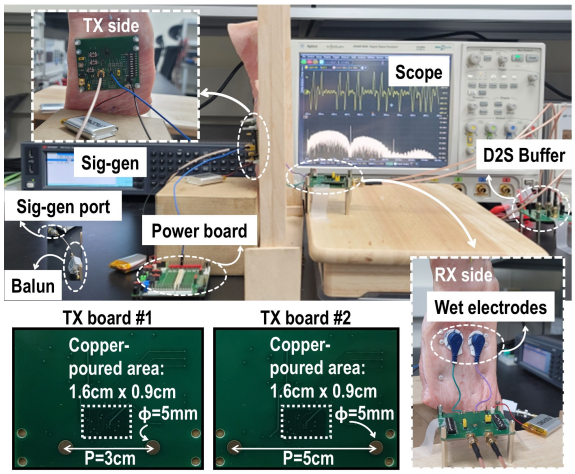

Fig. 8. Overall in-vitro measurement setup.

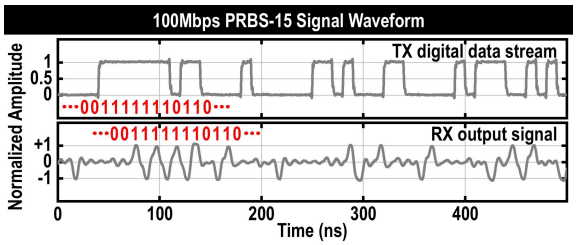

Fig. 9. Measured transmitted and received signal waveforms for a 100-Mbps PRBS-15 data stream.

Fig. 10 presents the eye diagrams measured under varying T and P conditions. As T increases from 10 mm to 15 mm and P decreases from 5 cm to 3 cm, the eye margin degrades due to decreased channel gain. Fig. 11 presents the bit-error-rate test (BERT) results measured at different electrode pitches and transmitted current amplitudes. At T = 15 mm and P = 3 cm, no bit error was measured for a total of 10^6 bits with TX power consumption of 112.2 μW. Fig. 12 summarizes and compares the performance of the proposed work with prior wireless neural implants along with the fabricated chip's die micrograph. This work achieves the highest TX energy efficiency with 0.94 pJ/b at T = 10 mm and 1.12 pJ/b at T = 15 mm, both measured with P = 3 cm and exhibiting a bit-error rate (BER) lower than 10^{-6} at a data rate of 100 Mb/s. The proposed IC was fabricated using a 65-nm CMOS process.

The performance comparison with prior implanted TXs and their external RXs is summarized in Table I. This work

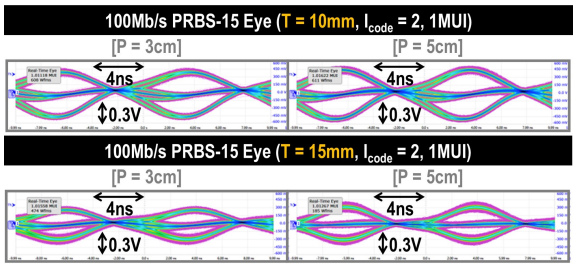

Fig. 10. Measured eye diagrams at different tissue thicknesses and electrode pitches.

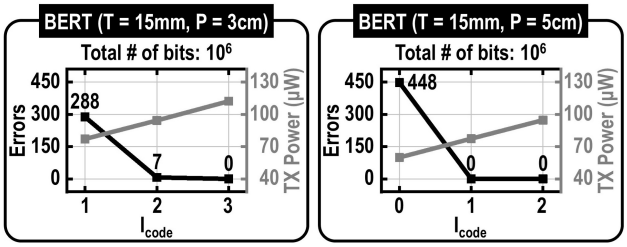

Fig. 11. Measured BER at different electrode pitches and transmitted current amplitudes.

achieves the best TX energy efficiency while offering significant merits such as RX implementation, low BER, and operation with thick tissue layers. Since the RX is placed outside the body, its power consumption is less critical. The RX is designed to consume 14.7 mW, which can be sufficiently supplied externally.

IV. Conclusion

This work presents a novel GCC scheme that overcomes key limitations of conventional approaches. By transmitting regulated current and receiving it through an active low-impedance input stage, the proposed architecture achieves simultaneous improvements in channel bandwidth, channel current gain, and RX sensitivity. The current-mode TX and RX front-ends enable efficient and robust uplink communication, making this approach well-suited for fully implantable neural systems requiring high-speed and low-power operation.

Acknowledgement

The chip fabrication and CAD tools were supported by the IC Design Education Center (IDEC), Korea. This work was supported by Samsung Electronics under Grant IO201209-07925-01 and the Ministry of Science and ICT (MSIT), Korea, under Grant 2022M3C1A3091627. The authors thank Yeseul Jeon for providing helpful comments throughout the research.

References

[1] M. Song *et al.*, "A 1.66 Gb/s and 5.8 pJ/b transcutaneous IR-UWB telemetry system with hybrid impulse modulation for intracortical brain-computer interfaces," in *IEEE International Solid-State Circuits Conference (ISSCC) Dig. Tech. Papers*, 2022, pp. 394–396.

[2] J. Lei *et al.*, "A 1.8 Gb/s, 2.3 pJ/bit, crystal-less IR-UWB transmitter for neural implants," in *IEEE International Solid-State Circuits Conference (ISSCC) Dig. Tech. Papers*, 2023, pp. 464–466.

[3] C. Lee *et al.*, "A miniaturized wireless neural implant with body-coupled data transmission and power delivery for freely behaving animals," in *IEEE International Solid-State Circuits Conference (ISSCC) Dig. Tech. Papers*, vol. 65, 2022, pp. 1–3.

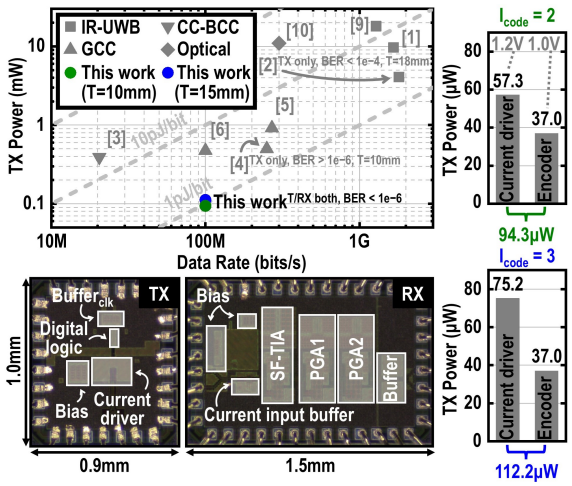

Fig. 12. Performance comparison with prior wireless neural implant TXs, along with die micrograph

TABLE I
Performance Comparison with State-of-the-Art Works.

	ISSCC 2023 [2]	ISSCC 2022 [3]	TMTT 2022 [4]	TBCAS 2024 [5]	VLSI 2019 [6]	This work	
Technology [nm]	40	180	28	65	180	65	
Wireless method	IR-UWB	CC-BCC	V_{TX}-V_{RX} GCC	V_{TX}-V_{RX} GCC	I_{TX}-V_{RX} GCC	I_{TX}-I_{RX} GCC	
Data rate [bit/s]	1.8G	20.48M	250M	270M	100M	100M	
Bit error rate	$<10^{-4}$	N.A.	2.4×10^{-6}	$<10^{-6}$	10^{-9}	$<10^{-6}$	
Test method	Porcine w/ skin	Rat brain	Porcine w/o skin	Porcine w/o skin	Porcine w/ skin	Porcine w/ skin	
Tissue thick. [mm]	18	N.A.	10	7	10	10	15
TX power cons. [mW]	4.09	0.39	0.5	0.92	0.48	0.09	0.11
TX energy eff. [pJ/bit]	2.3	19.0	2.0	3.4	4.8	0.9	1.1
RX power cons. [mW]	N.A. (TX only)	0.09	N.A. (TX only)	1.00	2.68	14.70	

[4] C. Shi *et al.*, "Galvanic-coupled trans-dural data transfer for high-bandwidth intracortical neural sensing," *IEEE Transactions on Microwave Theory and Techniques*, vol. 70, no. 10, pp. 4579–4589, 2022.

[5] C. Shi et al., "A spatially diverse 2TX-3RX galvanic-coupled transdural telemetry for tether-less distributed brain–computer interfaces," *IEEE Transactions on Biomedical Circuits and Systems*, vol. 18, no. 5, pp. 1014–1023, 2024.

[6] Y. Jeon *et al.*, "A 100Mb/s galvanically-coupled body-channel-communication transceiver with 4.75 pJ/b TX and 26.8 pJ/b RX for bionic arms," in *Proc. Symposium on VLSI Circuits*, Kyoto, Japan, 2019, pp. C292–C293.

[7] J. K. Lee *et al.*, "IIP2-improved frontend receiver using a mismatch compensation LNA," *Journal of Semiconductor Technology and Science*, vol. 17, no. 5, pp. 603–610, 2017.

[8] S. Yun *et al.*, "A 2.4/5 GHz dual-band low-noise and highly linear receiver with a new power-efficient feedforward OPAMP for WiFi-6 applications," *IEEE Access*, vol. 11, pp. 137 264–137 273, 2023.

[9] G. Lee *et al.*, "A 6–9 GHz 1.28 Gbps 76 mW amplitude and synchronized time shift keying IR-UWB CMOS transceiver for brain computer interfaces," *IEEE Transactions on Biomedical Circuits and Systems*, pp. 1–11, 2024.

[10] A. D. Marcellis *et al.*, "A 300 Mbps 37 pJ/bit pulsed optical biotelemetry," *IEEE Transactions on Biomedical Circuits and Systems*, vol. 14, no. 3, pp. 441–451, 2020.